Evolution of Two Cylindrical Vortex Sheets

by

Jeremy David Johnson

Undergraduate Honors Thesis

Department of Mathematics, University of New Mexico

Albuquerque, New Mexico

July 2007

Abstract

The evolution of two cylindrical vortex sheets are studied and numerically computed. The initial conditions, evolution equations, numerical methods needed (including integral approximations, correction terms, fourier filter implementation), numerical results, and an analysis of the results, as well as the time and nature of the singularity formation, are provided/explored.

Acknowledgments

Thanks to Professor Monika Nitsche for working with me on this research, and for providing me with a year long course of study in computational fluid mechanics. Thanks to student Roman Wowk for learning and researching along side of me. Also, thanks for support from the National Science Foundation REU.

.

Contents

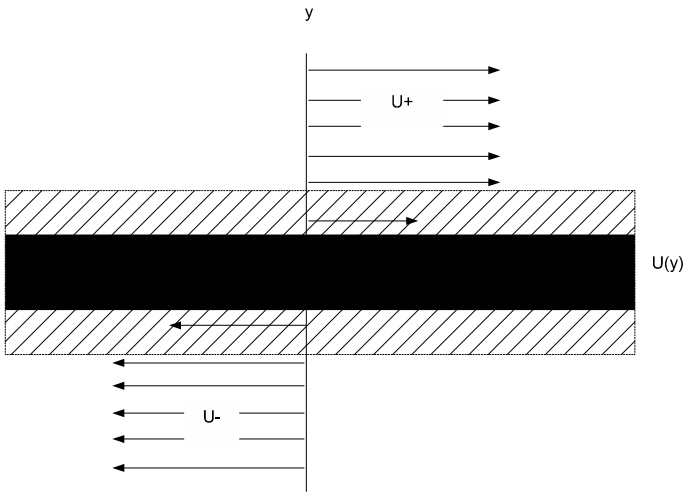

Fig. 0.1. A shear layer

Introduction

The evolution and singularity formation in a cylindrical vortex sheet has been studied and modeled [10]. The aim of this work seeks to extend the case of one cylindrical vortex sheet to that of two cylindrical vortex sheets.

Let two cylinders immersed in an inviscid fluid be given an impulse in a direction normal to itself. The resulting potential flow is induced by two planar vortex sheets in place of the two cylinders. Essentially, we let the cylinders instantaneously disappear, with a shear layer (figure 0.1) of zero thickness remaining. This surface is termed a vortex sheet (figure 0.2). Note that a vortex sheet has a discontinuous tangential velocity across the surface. The vorticity of the flow is defined as $\xi = \nabla \times \mathbf{u}$, where $\mathbf{u}$ is the velocity

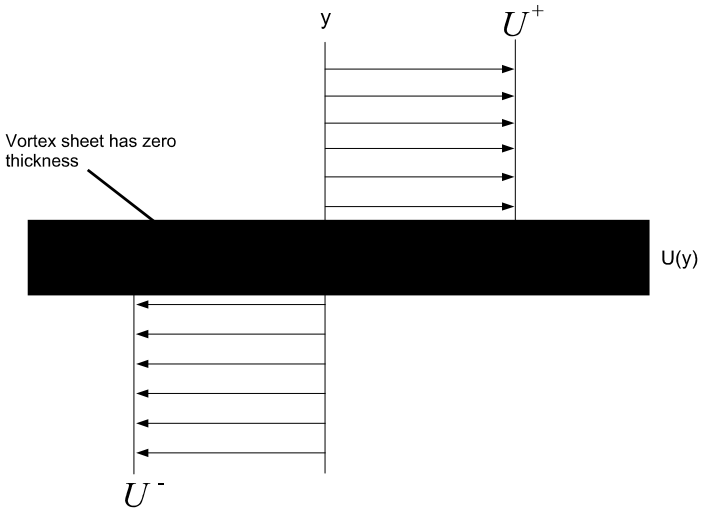

Fig. 0.2. Vortex sheet approximation

of the flow. ξ away from a vortex sheet is zero, yet $\int_S \xi \, da \neq 0$. In other words, ξ is a delta-function on the surface of the sheet.

The evolution of these two vortex sheets through time are studied. The governing equations, evolution equations, numerical methods needed (including integral approximations, correction terms, fourier filter implementation), numerical results, and an analysis of the results are provided. Furthermore, the

The initial conditions, evolution equations, numerical methods needed (including discretization, integral approximations, correction terms, fourier filter implementation), numerical results, and an analysis of the results are presented. Furthermore, the time and nature of singularity formation are examined.

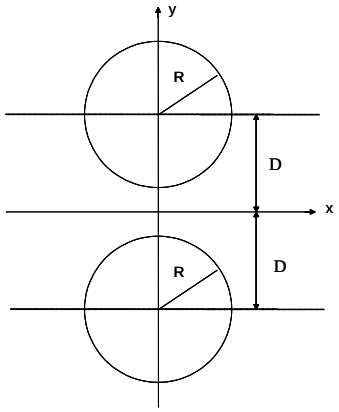

Fig. 1.3. Cross section

Chapter 1
Problem Formulation

1.1 Initial Conditions

Consider two identical cylindrical vortex sheets whose axies are z-directed and have radii R. Let their centers fall on the y-axis and be a distance D from the x-axis (figure 1.3). Then the cross section of the top cylinder can be described by the curve $(x(\alpha,t), y(\alpha,t))$, where $x(\alpha,t) = R\cos\alpha$, $y(\alpha,t) = D + R\sin\alpha$, and $\alpha \in [0, 2\pi]$. Suppose that $D > R$.

Let σ denote the vortex sheet strength and $\Gamma(\alpha)$ denote the circulation. Then σ is the jump in the tangential velocity across the sheet, and $\sigma(s,t) = \frac{\partial\Gamma}{\partial s}$, where s is the arclength.

1.2 Evolution Equations

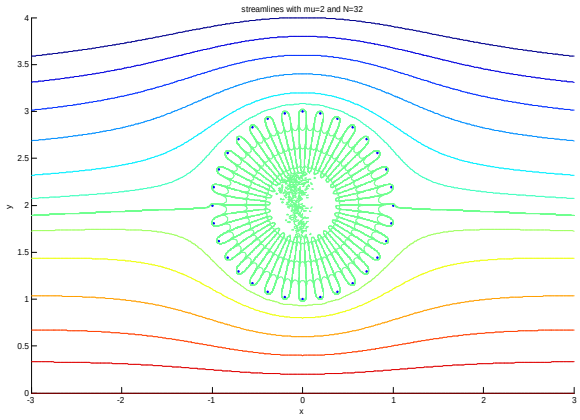

Fig. 1.4. With background velocity $\mathbf{u}_\infty = (U_\infty, 0)$.

Consider incompressible potential flow. Then for a point vortex at $\mathbf{x}_k$ and of strength Γ_k, the stream function at position $\mathbf{x}$ is given by $\psi_k(\mathbf{x}) = \frac{-\Gamma_k}{2\pi} \log \|\mathbf{x} - \mathbf{x}_k\|$. The velocity is $\mathbf{u}(\mathbf{x}) = \left(\frac{\psi_k(\mathbf{x})}{\partial y}, -\frac{\psi_k(\mathbf{x})}{\partial x}\right) = \left(-\frac{\Gamma_k}{2\pi}\left(\frac{y-y_k}{(x-x_k)^2+(y-y_k)^2}\right), -\frac{\Gamma_k}{2\pi}\left(\frac{x-x_k}{(x-x_k)^2+(y-y_k)^2}\right)\right)$. Now if we consider the contribution from N point vorticies in a plane, then by superposition, and since Γ_k is Lagrangian (invarient in time), $\mathbf{u}(\mathbf{x},t) = \sum_{k=1}^{N} \mathbf{u}_j(\mathbf{x},t)$

$= \sum_{k=1}^{N} \left(-\frac{\Gamma_k}{2\pi}\left(\frac{y-y_k}{(x-x_k)^2+(y-y_k)^2}\right), -\frac{\Gamma_k}{2\pi}\left(\frac{x-x_k}{(x-x_k)^2+(y-y_k)^2}\right)\right)$. Thus a set of N point vorticies moves at x_j, for $j = 1, ..., N$ moves according to

$\left(\frac{dx_j}{dt}, \frac{dy_j}{dt}\right) = \sum_{\substack{k=1 \\ k\neq j}}^{N} \left(-\frac{\Gamma_k}{2\pi}\left(\frac{y_j-y_k}{(x_j-x_k)^2+(y_j-y_k)^2}\right), -\frac{\Gamma_k}{2\pi}\left(\frac{x_j-x_k}{(x_j-x_k)^2+(y_j-y_k)^2}\right)\right)$ [2]. The $k = j$ term is not included in the summation so as to not include the self-contribution. Also, note that the term would be singular if this term was to be included. Let the given sheet be approximated by N vorticies, and let $N \to \infty$ and $\Delta\Gamma \to 0$. Then for a point on the sheet we get $\mathbf{u}(\mathbf{x},t) = \frac{1}{2\pi} P.V. \int_C \left(-\frac{y-\tilde{y}}{(x-\tilde{x})^2+(y-\tilde{y})^2}, \frac{x-\tilde{x}}{(x-\tilde{x})^2+(y-\tilde{y})^2}\right) d\tilde{\Gamma}$, where $d\Gamma = \Gamma'(\tilde{\alpha})\ d\tilde{\alpha}$ ([10]).

Consider the two cylindrical vortex sheets mentioned above. Let us approximate each sheet by N uniformly spaced point vorticies. Then at some point vortex of position $\mathbf{x}_j$, we have

$\psi(\mathbf{x}_j) = \frac{-1}{2\pi} \sum_{\substack{k=1 \\ k\neq j}}^{N} \Gamma_k \log\sqrt{(x_j - x_k)^2 + (y_j - y_k)^2}$

$-\frac{1}{2\pi} \sum_{k=1}^{N} \Gamma_k^B \log\sqrt{(x_j - x_k^B)^2 + (y_j - y_k^B)^2}$, where $\left(x_k^B, y_k^B\right)$ and Γ_k^B denote a point and the corresponding circulation on the bottom sheet, respectively. Notice that $\left(x_k^B, y_k^B\right) = (x_k, -y_k)$ and $\Gamma_k^B = -\Gamma_k$. Thus, $\psi(\mathbf{x}_j) = \frac{-1}{2\pi} \sum_{\substack{k=1 \\ k\neq j}}^{N} \Gamma_k \log\sqrt{(x_j - x_k)^2 + (y_j - y_k)^2} + \frac{1}{2\pi} \sum_{k=1}^{N} \Gamma_k^B \log\sqrt{(x_j - x_k)^2 + (y_j + y_k)^2}$. Again using $\mathbf{u}(\mathbf{x}) = \left(\frac{\psi_k(\mathbf{x})}{\partial y}, -\frac{\psi_k(\mathbf{x})}{\partial x}\right)$, and letting $N \to \infty$ and $\Delta\Gamma \to 0$, it follows that $\frac{dx_j}{dt} = -\frac{1}{2\pi} P.V. \int_C \frac{y-\tilde{y}}{(x-\tilde{x})^2+(y-\tilde{y})^2} d\tilde{\Gamma} + \frac{1}{2\pi} \int_C \frac{y+\tilde{y}}{(x-\tilde{x})^2+(y+\tilde{y})^2} d\tilde{\Gamma}$, $\frac{dy_j}{dt} = \frac{1}{2\pi} P.V. \int_C \frac{x-\tilde{x}}{(x-\tilde{x})^2+(y-\tilde{y})^2} d\tilde{\Gamma} - \frac{1}{2\pi} \int_C \frac{x-\tilde{x}}{(x-\tilde{x})^2+(y+\tilde{y})^2} d\tilde{\Gamma}$.

Note that we assummed the background velocity of the flow $\mathbf{u}_\infty = \mathbf{0}$.

1.4 shows the streamlines, or level curves, of ψ with a background velocity $\mathbf{u}_\infty = (U_\infty, 0)$. In this case, $\psi_{mov}(x, y) = \psi(x, y) - U_\infty y$,

and thus, $\mathbf{u}_{mov}(\mathbf{x}) = \left(\frac{\psi_k(\mathbf{x})}{\partial y} - U_\infty, -\frac{\psi_k(\mathbf{x})}{\partial x}\right)$. Then

$\frac{dx_j}{dt} = -\frac{1}{2\pi} P.V. \int_C \frac{y-\tilde{y}}{(x-\tilde{x})^2+(y-\tilde{y})^2} d\tilde{\Gamma} + \frac{1}{2\pi} \int_C \frac{y+\tilde{y}}{(x-\tilde{x})^2+(y+\tilde{y})^2} d\tilde{\Gamma} - U_\infty$. Note that $\frac{dy_j}{dt}$ would still be the same as above.

Side note: in figure 1.4, the sparadic streamlines inside of the cylinder are simply noise due to roundoff error.

1.2.1 Non-dimensionalization

Let us change variables and introduce the following non-dimensional quantities, which we will denote by $(*)$:

Let R have units of length and U have units of velocity, $\frac{\text{length}}{\text{time}}$. Let us introduce the following dimensionless quantities $x^* = \frac{x}{R}$, $\tilde{x}^* = \frac{\tilde{x}}{R}$, $y^* = \frac{y}{R}$, $\tilde{y}^* = \frac{\tilde{y}}{R}$, $\Gamma^* = \frac{\Gamma}{RU}$, and $t^* = \frac{U}{R}t$.

So $Rx^* = x$, $Ry^* = y$, $\frac{dx}{dx^*} = R$, $\frac{dy}{dy^*} = R$, $d\Gamma = RU\ d\Gamma^*$,and $\frac{dt^*}{dt} = \frac{U}{R}$.

Then $Rx^* = x\left(\alpha, t\right) = R\cos\alpha$ implies that $x^* = \cos\alpha$. Similarly, $Ry^* = y\left(\alpha, t\right) = D + R\sin\alpha$ yields $y^* = \frac{D}{R} + \sin\alpha$.

Then using $\frac{dx(\alpha,t)}{dt} = \frac{dx}{dx^*}\frac{dx^*}{dt} = R\frac{dx^*}{dt} = R\frac{dx^*}{dt^*}\frac{dt^*}{dt} = R\frac{U}{R}\frac{dx^*}{dt^*} = U\frac{dx^*}{dt^*}$, we get

$$\frac{dx^*}{dt^*} = \frac{1}{U}\left[U\frac{dx^*}{dt^*}\right] = \frac{1}{U}\frac{dx(\alpha,t)}{dt}$$

$$= \frac{1}{U}\left[-\frac{1}{2\pi}P.V.\int_0^{2\pi}\frac{y-\tilde{y}}{(x-\tilde{x})^2+(y-\tilde{y})^2}\frac{d\Gamma}{d\tilde{\alpha}}d\tilde{\alpha} + \frac{1}{2\pi}\int_0^{2\pi}\frac{y+\tilde{y}}{(x-\tilde{x})^2+(y+\tilde{y})^2}\frac{d\Gamma}{d\tilde{\alpha}}d\tilde{\alpha}\right]$$

$$= \frac{-1}{2\pi U}P.V.\int_0^{2\pi}\left[\frac{y-\tilde{y}}{(x-\tilde{x})^2+(y-\tilde{y})^2}\right]\frac{d\Gamma}{d\tilde{\alpha}}d\tilde{\alpha} + \frac{1}{2\pi U}\int_0^{2\pi}\left[\frac{y+\tilde{y}}{(x-\tilde{x})^2+(y+\tilde{y})^2}\right]\frac{d\Gamma}{d\tilde{\alpha}}d\tilde{\alpha}$$

$$= \frac{-1}{2\pi U}P.V.\int_0^{2\pi}\left[-\frac{Ry^*-R\tilde{y}^*}{(Rx^*-R\tilde{x}^*)^2+(Ry^*-R\tilde{y}^*)^2}\right]\frac{RU\ d\Gamma^*}{d\tilde{\alpha}}d\tilde{\alpha}$$

$$+\frac{1}{2\pi U}\int_0^{2\pi}\left[\frac{Ry^*+R\tilde{y}^*}{(Rx^*-R\tilde{x}^*)^2+(Ry^*+R\tilde{y}^*)^2}\right]\frac{RU\ d\Gamma^*}{d\tilde{\alpha}}d\tilde{\alpha}$$

$$= -\frac{R^2U}{2\pi R^2U}P.V.\int_0^{2\pi}\left[-\frac{y^*-\tilde{y}^*}{(x^*-\tilde{x}^*)^2+(y^*-\tilde{y}^*)^2}\right]\frac{d\Gamma^*}{d\tilde{\alpha}}d\tilde{\alpha}$$

$$+\frac{R^2U}{2\pi R^2U}\int_0^{2\pi}\left[\frac{y^*+\tilde{y}^*}{(x^*-\tilde{x}^*)^2+(y^*+\tilde{y}^*)^2}\right]\frac{d\Gamma^*}{d\tilde{\alpha}}d\tilde{\alpha}$$

$$= -\frac{1}{2\pi}\int_0^{2\pi}\left[\frac{y^*-\tilde{y}^*}{(x^*-\tilde{x}^*)^2+(y^*-\tilde{y}^*)^2}\right]\frac{d\Gamma^*}{d\tilde{\alpha}}d\tilde{\alpha} + \frac{1}{2\pi}\int_0^{2\pi}\left[\frac{y^*+\tilde{y}^*}{(x^*-\tilde{x}^*)^2+(y^*+\tilde{y}^*)^2}\right]\frac{d\Gamma^*}{d\tilde{\alpha}}d\tilde{\alpha}.$$

Similarly, using $\frac{dy(\alpha,t)}{dt} = \frac{dy}{dy^*}\frac{dy^*}{dt} = R\frac{dy^*}{dt} = R\frac{dy^*}{dt^*}\frac{dt^*}{dt} = R\frac{U}{R}\frac{dy^*}{dt^*} = U\frac{dy^*}{dt^*}$, it follows that

$$\frac{dy^*}{dt^*} = \frac{1}{U}\left[U\frac{dy^*}{dt^*}\right] = \frac{1}{U}\frac{dy(\alpha,t)}{dt}$$

$$= \frac{1}{U}\left[\frac{1}{2\pi}P.V.\int_0^{2\pi}\frac{x-\tilde{x}}{(x-\tilde{x})^2+(y-\tilde{y})^2}\frac{d\Gamma}{d\tilde{\alpha}}d\tilde{\alpha} - \frac{1}{2\pi}\int_0^{2\pi}\frac{x-\tilde{x}}{(x-\tilde{x})^2+(y+\tilde{y})^2}\frac{d\Gamma}{d\tilde{\alpha}}d\tilde{\alpha}\right]$$

$$= \frac{1}{2\pi U}P.V.\int_0^{2\pi}\left[\frac{x-\tilde{x}}{(x-\tilde{x})^2+(y-\tilde{y})^2}\right]\frac{d\Gamma}{d\tilde{\alpha}}d\tilde{\alpha} - \frac{1}{2\pi U}\int_0^{2\pi}\left[\frac{x-\tilde{x}}{(x-\tilde{x})^2+(y+\tilde{y})^2}\right]\frac{d\Gamma}{d\tilde{\alpha}}d\tilde{\alpha}$$

$$= \frac{1}{2\pi U}P.V.\int_0^{2\pi}\left[\frac{Rx^*-R\tilde{x}^*}{(Rx^*-R\tilde{x}^*)^2+(Ry^*-R\tilde{y}^*)^2}\right]\frac{RU}{}\frac{d\Gamma^*}{d\tilde{\alpha}}d\tilde{\alpha}$$

$$-\frac{1}{2\pi U}\int_0^{2\pi}\left[\frac{Rx^*-R\tilde{x}^*}{(Rx^*-R\tilde{x}^*)^2+(Ry^*+R\tilde{y}^*)^2}\right]\frac{RU}{}\frac{d\Gamma^*}{d\tilde{\alpha}}d\tilde{\alpha}$$

$$= \frac{R^2U}{2\pi R^2U}P.V.\int_0^{2\pi}\left[\frac{x^*-\tilde{x}^*}{(x^*-\tilde{x}^*)^2+(y^*-\tilde{y}^*)^2} - \frac{x^*-\tilde{x}^*}{(x^*-\tilde{x}^*)^2+(y^*+\tilde{y}^*)^2}\right]\frac{d\Gamma^*}{d\tilde{\alpha}}d\tilde{\alpha}$$

$$-\frac{R^2U}{2\pi R^2U}\int_0^{2\pi}\left[\frac{x^*-\tilde{x}^*}{(x^*-\tilde{x}^*)^2+(y^*+\tilde{y}^*)^2}\right]\frac{d\Gamma^*}{d\tilde{\alpha}}d\tilde{\alpha}$$

$$= \frac{1}{2\pi}P.V.\int_0^{2\pi}\left[\frac{x^*-\tilde{x}^*}{(x^*-\tilde{x}^*)^2+(y^*-\tilde{y}^*)^2}\right]\frac{d\Gamma^*}{d\tilde{\alpha}}d\tilde{\alpha}$$

$$-\frac{1}{2\pi}\int_0^{2\pi}\left[\frac{x^*-\tilde{x}^*}{(x^*-\tilde{x}^*)^2+(y^*+\tilde{y}^*)^2}\right]\frac{d\Gamma^*}{d\tilde{\alpha}}d\tilde{\alpha}.$$

Thus, the governing equations $\left(\frac{dx^*}{dt^*}, \frac{dy^*}{dt^*}\right)$ are the same as those for $\left(\frac{dx}{dt}, \frac{dy}{dt}\right)$, where $x^* = \cos\alpha$ and $y^* = \frac{D}{R} + \sin\alpha$. Let us introduce μ, where $\mu = \frac{D}{R}$. Also, let us now rename (x^*, y^*) as (x, y). Then we have $x = \cos\alpha$ and $y = \mu + \sin\alpha$. Then since $D > R$, we have $\mu > 1$.

1.2.2 Solving for initial sheet strength

We can discretize the governing equations as follows

$$u\left(x_j, y_j\right) = -\frac{1}{2\pi}\sum_{\substack{k=1\\k\neq j}}^{N}\frac{y_j-y_k}{(x_j-x_k)^2+(y_j-y_k)^2}\sigma_k\Delta s_k + \frac{1}{2\pi}\sum_{k=1}^{N}\frac{y_j+y_k}{(x_j-x_k)^2+(y_j+y_k)^2}\sigma_k\Delta s_k - U_\infty$$

and $v\left(x_j, y_j\right) = \frac{1}{2\pi}\sum_{\substack{k=1\\k\neq j}}^{N}\frac{x_j-x_k}{(x_j-x_k)^2+(y_j-y_k)^2}\sigma_k\Delta s_k - \frac{1}{2\pi}\sum_{k=1}^{N}\frac{x_j-x_k}{(x_j-x_k)^2+((y_j+y_k))^2}\sigma_k\Delta s_k - V_\infty,$

where the background velocity is given by $\mathbf{u}_\infty = (U_\infty, V_\infty)$. Let $\mathbf{u}_\infty = (U_\infty, 0)$. Now by choosing uniform spacing of the N point vortices, we have $\Delta s_k = \Delta s = \frac{2\pi}{N}$. The fluid velocity has a tangential component and a component normal the the vortex sheet.

It is this normal component that determines the sheet's evolution. Note tht the tangential caomponent simply determines how marker particles move along the sheet [10].

Let us dot the discretized velocities with its normal vector,

$\mathbf{n}(\mathbf{x}_j) = (\cos\alpha_j, \sin\alpha_j)$. So $\mathbf{u}(\mathbf{x}_j)\cdot\mathbf{n}(\mathbf{x}_j) = 0$.

$$\text{So } \Delta s\left(-\frac{1}{2\pi}\sum_{\substack{k=1\\k\neq j}}^{N}\frac{y_j-y_k}{(x_j-x_k)^2+(y_j-y_k)^2}\sigma_k+\frac{1}{2\pi}\sum_{k=1}^{N}\frac{y_j+y_k}{(x_j-x_k)^2+(y_j+y_k)^2}\sigma_k\right)\cos\alpha_j$$

$$+\Delta s\left(\frac{1}{2\pi}\sum_{\substack{k=1\\k\neq j}}^{N}\frac{x_j-x_k}{(x_j-x_k)^2+(y_j-y_k)^2}\sigma_k-\frac{1}{2\pi}\sum_{k=1}^{N}\frac{x_j-x_k}{(x_j-x_k)^2+((y_j+y_k))^2}\sigma_k\right)\sin\alpha_j$$

$= U_\infty\cos\alpha_j$. Now, since $\Delta s = \frac{2\pi}{N}$,

$$\frac{1}{N}\left(-\sum_{\substack{k=1\\k\neq j}}^{N}\frac{y_j-y_k}{(x_j-x_k)^2+(y_j-y_k)^2}\sigma_k+\sum_{j,k=1}^{N}\frac{y_j+y_k}{(x_j-x_k)^2+(y_j+y_k)^2}\sigma_k\right)\cos\alpha_j$$

$$+\frac{1}{N}\left(\sum_{\substack{k=1\\k\neq j}}^{N}\frac{x_j-x_k}{(x_j-x_k)^2+(y_j-y_k)^2}\sigma_k-\sum_{k=1}^{N}\frac{x_j-x_k}{(x_j-x_k)^2+(y_j+y_k)^2}\sigma_k\right)\sin\alpha_j$$

$= U_\infty\cos\alpha_j$.

Define

$$A_{jj} = \frac{1}{N}\left[\left(\frac{y_j+y_j}{(x_j-x_k)^2+(y_j+y_k)^2}\right)\cos\alpha_j+\left(-\frac{x_j-x_j}{(x_j-xj)^2+(y_j+y_j)^2}\right)\sin\alpha_j\right],$$

$$A_{jk} = \frac{1}{N}[\left(-\frac{y_j-y_k}{(x_j-x_k)^2+(y_j-y_k)^2}+\frac{y_j+y_k}{(x_j-x_k)^2+(y_j+y_k)^2}\right)\cos\alpha_j$$

$$+\left(\frac{x_j-x_k}{(x_j-x_k)^2+(y_j-y_k)^2}-\frac{x_j-x_k}{(x_j-x_k)^2+(y_j+y_k)^2}\right)\sin\alpha_j] \text{ for } k\neq j, \text{ and}$$

$b_j = U_\infty\cos\alpha_j$.

Then we have $\begin{bmatrix} A_{11} & \dots & A_{1N}\\ A_{21} & \dots & A_{2N}\\ & \dots & \\ & \dots & \\ A_{N1} & \dots & A_{NN}\end{bmatrix}\begin{bmatrix}\sigma_1\\.\\.\\.\\\sigma_N\end{bmatrix} = \begin{bmatrix}U_\infty\cos\alpha_1\\.\\.\\.\\U_\infty\cos\alpha_N\end{bmatrix}$, that is, $A\boldsymbol{\sigma} = \mathbf{b}$.

Initially, we know A and $\mathbf{b}$. So we can find $\boldsymbol{\sigma}$, which was originally computed in Matlab via the command $\boldsymbol{\sigma} = A\backslash\mathbf{b}$.

Now, there is not convergence of the $\boldsymbol{\sigma}$'s as N is increased (figure 1.2.2).

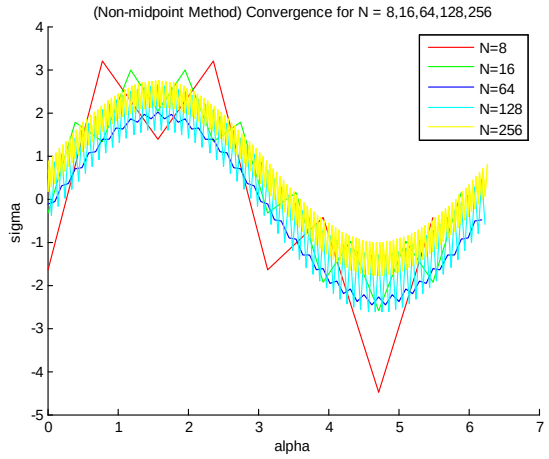

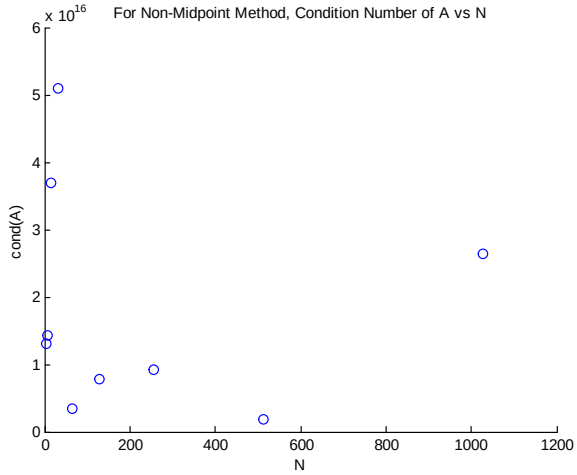

Also, note that condition number of A is very large (figure 1.2.2), and thus, A is poorly conditioned. Matlab gives the following error: *Matrix is close to singular or badly scaled. Results may be inaccurate.*

1.2.3 Midpoint Method

Let $\left(x_j^m, y_j^m\right) = \left(\cos\alpha_j^m, \mu + \sin\alpha_j^m\right)$, where $\alpha_j^m = \alpha_j + \frac{\pi}{N}$. Remember that N is again the number of point vortices. So $\left(x_j^m, y_j^m\right)$ is the "midpoint" between two adjacent point

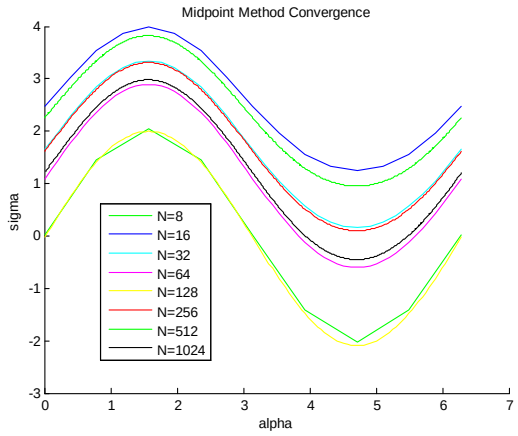

vortices. Evaluate the velocities $\mathbf{u}$ at $\mathbf{u}\left(x_j^m, y_j^m\right)$ instead of at (x_j, y_j). $u\left(x_j^m, y_j^m\right) = -\frac{1}{2\pi}\sum_{k=1}^{N}\frac{y_j^m - y_k}{\left(x_j^m - x_k\right)^2 + \left(y_j^m - y_k\right)^2}\sigma_k \Delta s_k + \frac{1}{2\pi}\sum_{k=1}^{N}\frac{y_j^m + y_k}{\left(x_j^m - x_k\right)^2 + \left(y_j^m + y_k\right)^2}\sigma_k \Delta s_k - U_\infty$ and $v\left(x_j, y_j\right) = \frac{1}{2\pi}\sum_{k=1}^{N}\frac{x_j - x_k}{(x_j - x_k)^2 + (y_j - y_k)^2}\sigma_k \Delta s_k - \frac{1}{2\pi}\sum_{k=1}^{N}\frac{x_j - x_k}{(x_j - x_k)^2 + ((y_j + y_k))^2}\sigma_k \Delta s_k - V_\infty$. The $k \neq j$ constraint in the first summations is now excluded. We again take $\mathbf{u}\left(\mathbf{x}_j^m\right) \cdot \mathbf{n}\left(\mathbf{x}_j^m\right) = 0$, where now we have $\mathbf{n}\left(\mathbf{x}_j^m\right) = \left(\cos\alpha_j^m, \sin\alpha_j^m\right)$ is the normal vector at the midpoint $\mathbf{x}_j^m$. Dot the discretized velocities with its normal vector, $\mathbf{n}\left(\mathbf{x}_j\right) = \left(\cos\alpha_j, \sin\alpha_j\right)$. So $\mathbf{u}\left(\mathbf{x}_j\right) \cdot \mathbf{n}\left(\mathbf{x}_j\right) = 0$.

Define

$A_{jk} = \frac{1}{N}\left[\left(-\frac{y_j^m - y_k}{\left(x_j^m - x_k\right)^2 + \left(y_j^m - y_k\right)^2} + \frac{y_j^m + y_k}{\left(x_j^m - x_k\right)^2 + \left(y_j^m + y_k\right)^2}\right)\cos\alpha_j + \left(\frac{x_j^m - x_k}{\left(x_j^m - x_k\right)^2 + \left(y_j^m - y_k\right)^2} - \frac{x_j^m - x_k}{\left(x_j^m - x_k\right)^2 + \left(y_j^m + y_k\right)^2}\right)\sin\alpha_j^m\right]$, and

$b_j = U_\infty \cos\alpha_j^m$. Then we again have the system $A\boldsymbol{\sigma} = \mathbf{b}$. A has a little bit better condition number (figure **??**). This is due to $\left(x_j^m - x_k\right)^2 + \left(y_j^m - y_k\right)^2$ being not quite as small as $(x_j - x_k)^2 + (y_j - y_k)^2$, for some certain values of j, k. Yet, matlab still gives the following error: *Matrix is close to singular or badly scaled. Results may be inaccurate*. Again, there is not convergence of the $\boldsymbol{\sigma}$'s as N is increased (figure 1.2.3).

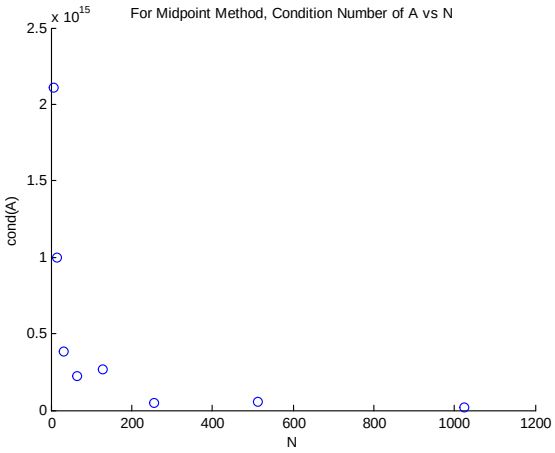

1.2.4 Zero Total Circulation Constraint

Let us use the midpoint method with the additional constraint that the total circulation is zero, $\Gamma_{\text{Total}} = 0$. Note that $\Gamma_{\text{Total}} = \sum_{k=1}^{N} \sigma_k \Delta s_k = \Delta s \sum_{k=1}^{N} \sigma_k$, where again $\Delta s_k = \Delta s = \frac{2\pi}{N}$.

Define $A_{jk} = \frac{1}{N} \left[\begin{array}{l} \left(-\frac{y_j^m - y_k}{\left(x_j^m - x_k\right)^2 + \left(y_j^m - y_k\right)^2} + \frac{y_j^m + y_k}{\left(x_j^m - x_k\right)^2 + \left(y_j^m + y_k\right)^2} \right) \cos\alpha_j \\ + \left(\frac{x_j^m - x_k}{\left(x_j^m - x_k\right)^2 + \left(y_j^m - y_k\right)^2} - \frac{x_j^m - x_k}{\left(x_j^m - x_k\right)^2 + \left(y_j^m + y_k\right)^2} \right) \sin\alpha_j^m \end{array} \right]$

if $j \neq N+1$,

and $A_{jk} = \Delta s$, if $j = N+1$, as well as

$b_j = \left\{ \begin{array}{c} U_\infty \cos\alpha_j, \text{ if } j \neq N+1 \\ 0, \text{ if } j = N+1 \end{array} \right.$.

Then we have the system $\left[\begin{array}{ccc} A_{11} & \ldots & A_{1N} \\ A_{21} & \ldots & A_{2N} \\ & \cdots & \\ & \cdots & \\ A_{N1} & \ldots & A_{NN} \\ \Delta s & \ldots & \Delta s \end{array} \right] \left[\begin{array}{c} \sigma_1 \\ . \\ . \\ . \\ \sigma_N \end{array} \right] = \left[\begin{array}{c} U_\infty \cos\alpha_1 \\ . \\ . \\ . \\ U_\infty \cos\alpha_N \\ 0 \end{array} \right]$, or again, $A\boldsymbol{\sigma} = \mathbf{b}$. This system is overdetermined, and must be solved in the least squares sense. The $\boldsymbol{\sigma}$'s were originally computed in Matlab using the command $\boldsymbol{\sigma} = A \backslash \mathbf{b}$ for the preliminary results. Yet, the $\boldsymbol{\sigma}$'s were later computed in fortran with the aid of the subroutine

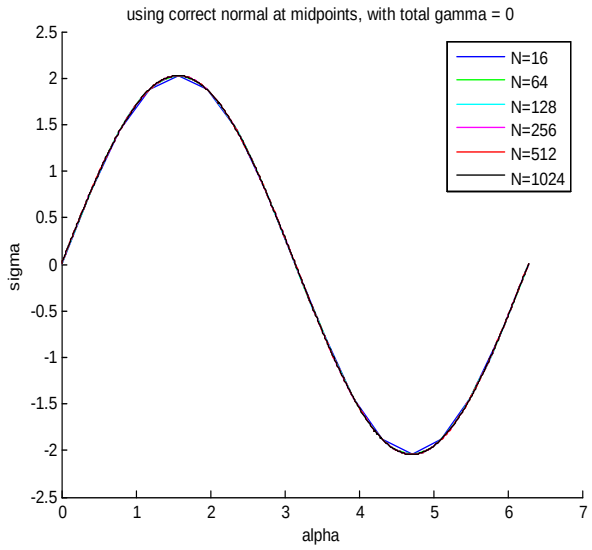

HFTI which was downloaded from netlib [7], and originally published and commented upon in the text [6]. This implementation in fortran was performed so that $\boldsymbol{\sigma}$'s could be computed quickly with N large for a variety of μ values. HFTI provides a solution of the least squares problem by housholder transformations.

For this case, there is convergence of the $\boldsymbol{\sigma}$'s as N is increased (figures 1.2.4, 1.2.4). Also note the good condition number of A (figure 1.2.4).

See figure 1.2.4 to observe how $\boldsymbol{\sigma}$ varies for different μ. As $\mu \to 1$, $\boldsymbol{\sigma}$ starts to blow up at $\alpha = \frac{3\pi}{2} \approx 4.712\,4$. Also note that as μ increases, $\sigma(\alpha) \to \sin(\alpha)$, which is consistent with the limiting case of one cylindrical vortex sheet, which was studied by [10].

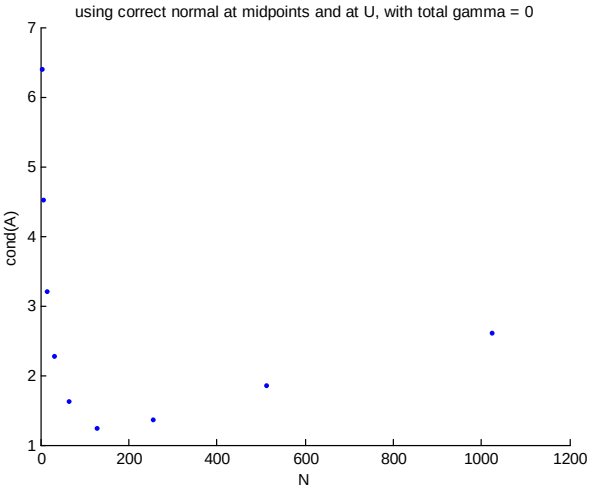
using correct normal at midpoints and at U, with total gamma = 0
cond(A)
N
1
2
3
4
5
6
7
0
200
400
600
800
1000
1200

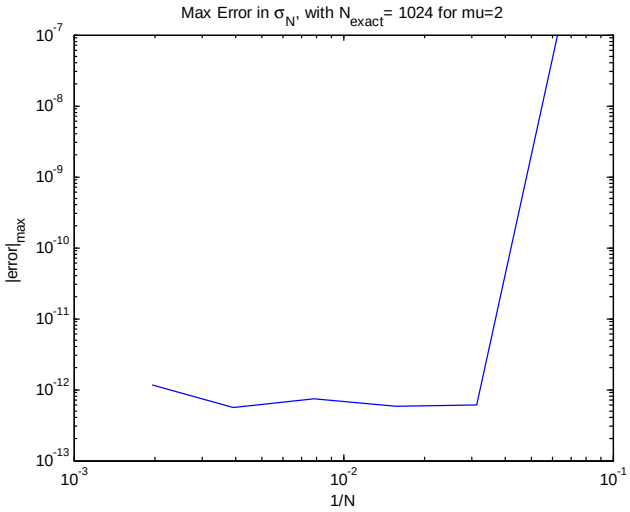
Max Error in σN, with Nexact= 1024 for mu=2
|error|max
1/N
10-7
10-8
10-9
10-10
10-11
10-12
10-13
10-3
10-2
10-1

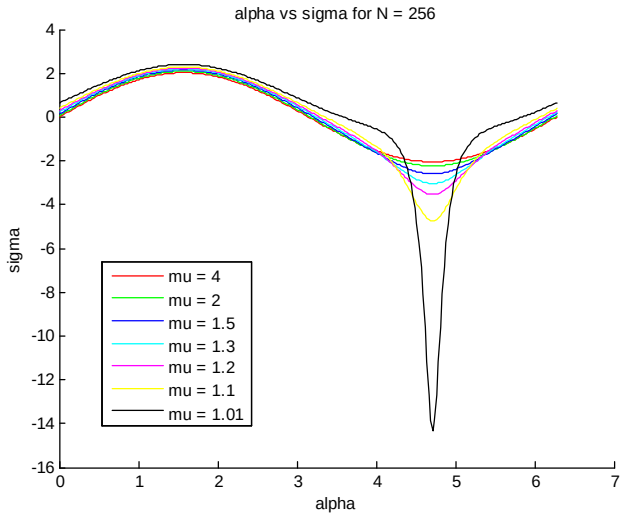
alpha vs sigma for N = 256
sigma
alpha
4
2
0
-2
-4
-6
-8
-10
-12
-14
-16
0
1
2
3
4
5
6
7
mu = 4
mu = 2
mu = 1.5
mu = 1.3
mu = 1.2
mu = 1.1
mu = 1.01

Chapter 2
Numerical Methods

2.1 Overview

The cylindrical vortex sheets are discretized each by N point vortices, at $(x_j, y_j) = (x(\alpha_j), y_j(\alpha_j))$, with a uniform mesh $\alpha_j = (j-1)h$, where $h = \frac{2\pi}{N}$. Remember that we have shown

$$\frac{dx_j}{dt}$$

$$= \frac{-1}{2\pi} P.V. \int_0^{2\pi} \frac{y_j - y(\alpha)}{(x_j - x(\alpha))^2 + (y_j - y(\alpha))^2} \Gamma'(\alpha)\, d\alpha + \frac{1}{2\pi} \int_0^{2\pi} \frac{y_j + y(\alpha)}{(x_j - x(\alpha))^2 + (y_j + y(\alpha))^2} \Gamma'(\alpha)\, d\alpha$$

and $v(x_j, y_j) = v_j = \frac{dy_j}{dt} = \frac{1}{2\pi} P.V. \int_0^{2\pi} \frac{x_j - x(\alpha)}{(x_j - x(\alpha))^2 + (y_j - y(\alpha))^2} \Gamma'(\alpha)\, d\alpha$

$$- \frac{1}{2\pi} \int_0^{2\pi} \frac{x_j - x(\alpha)}{(x_j - x(\alpha))^2 + (y_j + y(\alpha))^2} \Gamma'(\alpha)\, d\alpha.$$

Let $u_j = u(x_j, y_j) = \frac{dx_j}{dt}$, $v_j = v(x_j, y_j) = \frac{dy_j}{dt}$. Also, define $G^u(\alpha) = \frac{y_j - y(\alpha)}{(x_j - x(\alpha))^2 + (y_j - y(\alpha))^2}$ and $G^v(\alpha) = \frac{x_j - x(\alpha)}{(x_j - x(\alpha))^2 + (y_j - y(\alpha))^2}$. The integrals given by $\left(\frac{dx_j}{dt}, \frac{dy_j}{dt}\right)$ will be approximated by the a quadrature rule. The system will then be integrated in time by a forth order Runge-Kutta method, and a Fourier filter will be applied.

2.1.1 Integral Approximations

The integrals expressing $\left(\frac{dx_j}{dt}, \frac{dy_j}{dt}\right)$ are approximated by the trapezoid rule (figure 2.5) [11]. The $j = k$ contribution is dropped in the principle-value integrals. This is a first-order approximation.

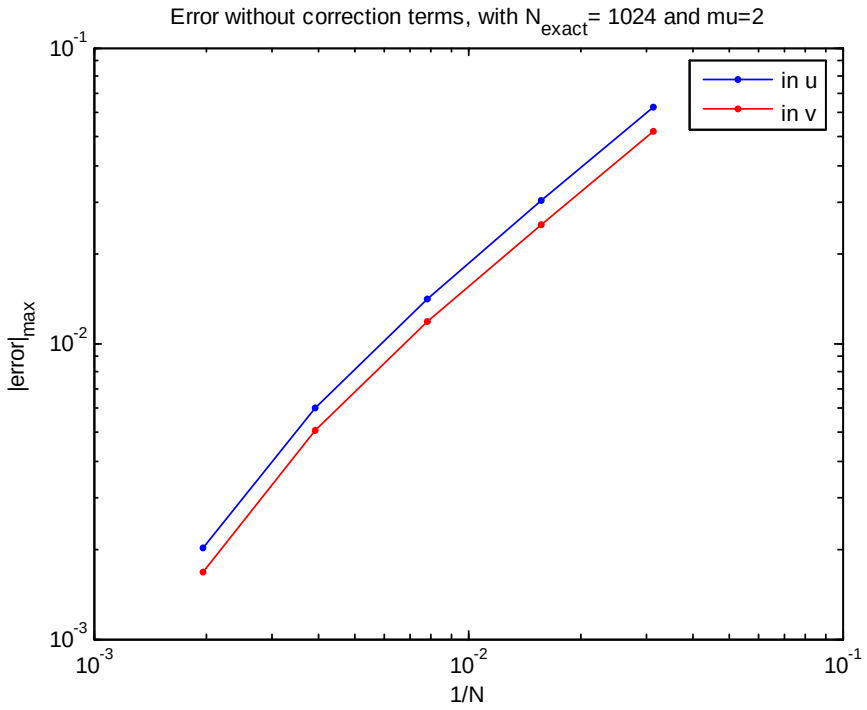

Fig. 2.5. Convergence of integrals using the trapezoid rule approximation

2.1.2 Correction Terms

For the principle value integrals, an additional correction term can be added, which is found via Taylor expansion.

Let $(x(\alpha), y(\alpha)) = (x, y)$, $(x(\alpha_j), y(\alpha_j)) = (x_j, y_j)$, and $h = \alpha - \alpha_j$.

Using Taylor series about $\alpha = \alpha_j$, we have

$x(\alpha) = x(\alpha_j) + x'(\alpha_j)(\alpha - \alpha_j) + \frac{x''(\alpha_j)}{2}(\alpha - \alpha_j)^2 + \ldots$,

$y(\alpha) = y(\alpha_j) + y'(\alpha_j)(\alpha - \alpha_j) + \frac{y''(\alpha_j)}{2}(\alpha - \alpha_j)^2 + \ldots$,

and $\Gamma'(\alpha) = \Gamma'(\alpha_j) + \Gamma''(\alpha_j)(\alpha - \alpha_j) + \ldots$.

Rewriting this, we have $x(\alpha) = x_j + x'_j h + \frac{x''_j}{2}h^2 + \ldots$, $y(\alpha) = y_j + y'_j h + \frac{y''_j}{2}h^2 + \ldots$, and $\Gamma'(\alpha) = \Gamma'_j + \Gamma''_j h + \ldots$.

So $G^u(\alpha) = \frac{y_j - y(\alpha)}{(x_j - x(\alpha))^2 + (y_j - y(\alpha))^2}\Gamma'(\alpha)$

$$= \frac{\left(y_j - \left[y_j + y'_j h + \frac{y''_j}{2}h^2 + O\left(h^3\right)\right]\right)\left[\Gamma'_j + \Gamma''_j h + O\left(h^2\right)\right]}{\left(x_j - \left[x_j + x'_j h + \frac{x''_j}{2}h^2 + O(h^3)\right]\right)^2 + \left(y_j - \left[y_j + y'_j h + \frac{y''_j}{2}h^2 + O(h^3)\right]\right)^2}$$

$$= \frac{\left[-y'_j h - \frac{y''_j}{2}h^2 + O\left(h^3\right)\right]\left[\Gamma'_j + \Gamma''_j h + O\left(h^2\right)\right]}{\left(x_j - \left[x_j + x'_j h + \frac{x''_j}{2}h^2 + O(h^3)\right]\right)^2 + \left(y_j - \left[y_j + y'_j h + \frac{y''_j}{2}h^2 + O(h^3)\right]\right)^2}$$

$$= \frac{\left[-y'_j h - \frac{y''_j}{2}h^2 + O\left(h^3\right)\right]\left[\Gamma'_j + \Gamma''_j h + O\left(h^2\right)\right]}{\left(-x'_j h - \frac{x''_j}{2}h^2 + O(h^3)\right)^2 + \left(-y'_j h - \frac{y''_j}{2}h^2 + O(h^3)\right)^2}$$

$$= \frac{-y'_j h\Gamma'_j + h^2\left(-\frac{y''_j}{2}\Gamma'_j - y'_j\Gamma''_j\right) + O\left(h^3\right)}{h^2\left(x_j^2 + y_j^2\right) + h^3\left(x'_j x''_j + y'_j y''_j\right) + O(h^4)} = \frac{-\frac{y'_j\Gamma'_j}{h} - \left(\frac{y''_j}{2}\Gamma'_j + y'_j\Gamma''_j\right) + O(h)}{\left(x_j^2 + y_j^2\right) + h\left(x'_j x''_j + y'_j y''_j\right) + O(h^2)}$$

$$= \frac{1}{x_j'^2 + y_j'^2}\left[1 - \frac{\left(x'_j x''_j + y'_j y''_j\right)h}{x_j'^2 + y_j'^2} + O\left(h^2\right)\right]\left[\frac{-y'_j\Gamma'_j}{h} - \frac{y''_j\Gamma_j}{2} - y'_j\Gamma''_j + O(h)\right],$$

and $G^v(\alpha) = \frac{x_j - x(\alpha)}{(x_j - x(\alpha))^2 + (y_j - y(\alpha))^2}\Gamma'(\alpha)$

$$= \frac{\left(x_j - \left[x_j + x'_j h + \frac{x''_j}{2}h^2 + O\left(h^3\right)\right]\right)\left[\Gamma'_j + \Gamma''_j h + O\left(h^2\right)\right]}{\left(x_j - \left[x_j + x'_j h + \frac{x''_j}{2}h^2 + O(h^3)\right]\right)^2 + \left(y_j - \left[y_j + y'_j h + \frac{y''_j}{2}h^2 + O(h^3)\right]\right)^2}$$

$$= \frac{\left[-x'_j h - \frac{x''_j}{2}h^2 + O\left(h^3\right)\right]\left[\Gamma'_j + \Gamma''_j h + O\left(h^2\right)\right]}{\left(x_j - \left[x_j + x'_j h + \frac{x''_j}{2}h^2 + O(h^3)\right]\right)^2 + \left(y_j - \left[y_j + y'_j h + \frac{y''_j}{2}h^2 + O(h^3)\right]\right)^2}$$

$$= \frac{\left[-x'_j h - \frac{x''_j}{2}h^2 + O\left(h^3\right)\right]\left[\Gamma'_j + \Gamma''_j h + O\left(h^2\right)\right]}{\left(-x'_j h - \frac{x''_j}{2}h^2 + O(h^3)\right)^2 + \left(-y'_j h - \frac{y''_j}{2}h^2 + O(h^3)\right)^2}$$

$$= \frac{-x'_j h\Gamma'_j + h^2\left(-\frac{x''_j}{2}\Gamma'_j - x'_j\Gamma''_j\right) + O\left(h^3\right)}{h^2\left(x_j^2 + y_j^2\right) + h^3\left(x'_j x''_j + y'_j y''_j\right) + O(h^4)} = \frac{-\frac{x'_j\Gamma'_j}{h} - \left(\frac{x''_j}{2}\Gamma'_j + x'_j\Gamma''_j\right) + O(h)}{\left(x_j^2 + y_j^2\right) + h\left(x'_j x''_j + y'_j y''_j\right) + O(h^2)}$$

$$= \frac{1}{x_j'^2 + y_j'^2}\left[1 - \frac{\left(x'_j x''_j + y'_j y''_j\right)h}{x_j'^2 + y_j'^2} + O\left(h^2\right)\right]\left[-\frac{x'_j\Gamma'_j}{h} - \left(\frac{x''_j}{2}\Gamma'_j + x'_j\Gamma''_j\right) + O\left(h\right)\right],$$

where we have noted that

$$\left(-x'_j h - \tfrac{x''_j}{2}h^2\right)^2 + \left(-y'_j h - \tfrac{y''_j}{2}h^2\right)^2 = \left(x'_j h + \tfrac{x''_j}{2}h^2\right)^2 + \left(y'_j h + \tfrac{y''_j}{2}h^2\right)^2$$

$$= \left(x'_j h + \tfrac{x''_j}{2}h^2\right)^2 + \left(y'_j h + \tfrac{y''_j}{2}h^2\right)^2$$

$$= h^2 x_j'^2 + h^3 x'_j x''_j + \tfrac{1}{4}h^4 x_j''^2 + h^2 y_j'^2 + h^3 y'_j y''_j + \tfrac{1}{4}h^4 y_j''^2$$

$$= h^2\left(x_j'^2 + y_j'^2\right) + h^3\left(x'_j x''_j + y'_j y''_j\right) + \tfrac{1}{4}h^4\left(x_j''^2 + y_j''^2\right)$$

$$= h^2\left(x_j'^2 + y_j'^2\right) + h^3\left(x'_j x''_j + y'_j y''_j\right) + O\left(h^4\right), \text{ and}$$

$$\frac{1}{\left(x_j^2 + y_j^2\right) + h\left(x'_j x''_j + y'_j y''_j\right) + O(h^3)} = \frac{1}{x_j'^2 + y_j'^2}\left(1 - \frac{\left(x'_j x''_j + y'_j y''_j\right)h}{x_j'^2 + y_j'^2} + O\left(h^2\right)\right).$$

Now, let $G^u(\alpha, \alpha_j) = \frac{c^u_{-1}}{\alpha - \alpha_j} + c^u_0 + c^u_1(\alpha - \alpha_j) + \ldots$ and $G^v(\alpha, \alpha_j) = \frac{c^v_{-1}}{\alpha - \alpha_j} + c^v_0 + c^v_1(\alpha - \alpha_j) + \ldots$.

Then $c^u_0 = \frac{1}{x_j'^2 + y_j'^2}\left[\frac{y'_j\Gamma'_j\left(x'_j x''_j + y'_j y''_j\right)}{x_j'^2 + y_j'^2} - \frac{y''_j}{2}\Gamma'_j - y'_j\Gamma''_j\right]$ and

$c^v_0 = \frac{1}{x_j'^2 + y_j'^2}\left[\frac{x'_j\Gamma'_j\left(x'_j x''_j + y'_j y''_j\right)}{x_j'^2 + y_j'^2} - \frac{x''_j}{2}\Gamma'_j - x'_j\Gamma''_j\right]$,

where we have observed that $G^u(\alpha_j, \alpha_j) = c^u_0$ and $G^v(\alpha_j, \alpha_j) = c^v_0$.

The derivatives x'_j, y'_j, x''_j, y''_j, and Γ''_j are computed via spectral differentiation. Note that $\Gamma'_j = \sigma_j$.

With these correction terms, we get good convergence of $\left(\frac{dx_j}{dt}, \frac{dy_j}{dt}\right)$ as N is increased, even at times other than $t = 0$ (figures 2.1.2, 2.1.2). Note the better convergence

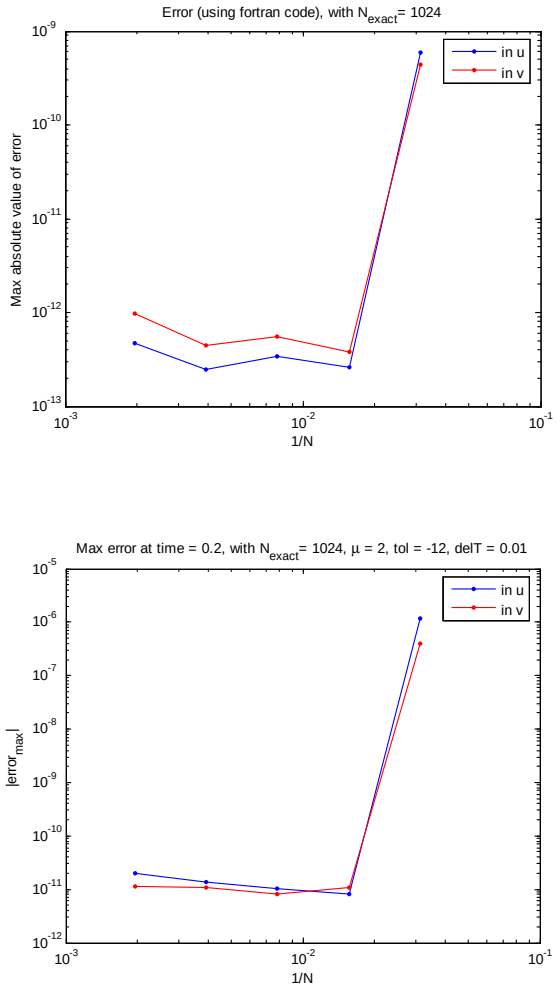

after the correction terms are added by comparing figures 2.1.2 and 2.1.2 with figure 2.5. Some of the higher error in 2.1.2 is do to newly introduced errors in the computed x_j, y_j positions as time evolves, imparted in part by a designated filter level. Yet, both figures illustrate exponential decay of the errors up within a magnitude of the filter level (see next section), which was 10^{-12} in this case.

2.1.3 Precision and a Fourier Filter

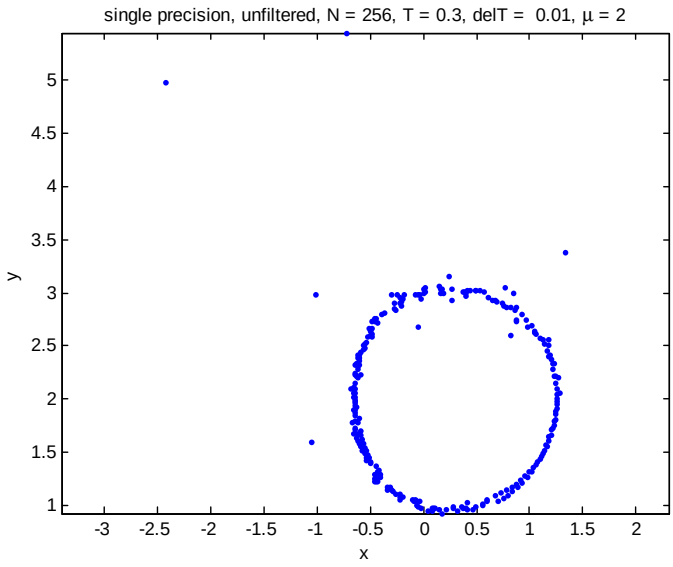

Simulations were performed in single precision, double precision, and double precision with the implementation of a fourier filter. Compare figures 2.1.3, 2.1.3, and 2.1.3. The noise is decreased when going from single to double precision, and when going from double precision to double precision with a fourier filter. See **??** for further explanation. The irregular point motion is caused in part by the machine's finite precision arithmetic. Methods for decreasing this irregualar point motion include using higher precision arithmetic, and/or by implementation of a fourier filter. Also, the noise is not do to a lack in resolution of time. This can be observed by comparing figures 2.1.3 and 2.1.3. The fourier filter is needed because high modes of error in $\mathbf{u}_j$ due to the discretization grow under the Kelvin-Hemholtz instability. The fourier filter level is set higher than values of the high modes times the timestep. For a given timestep, all of the modes below the designated filter level are set to 0.

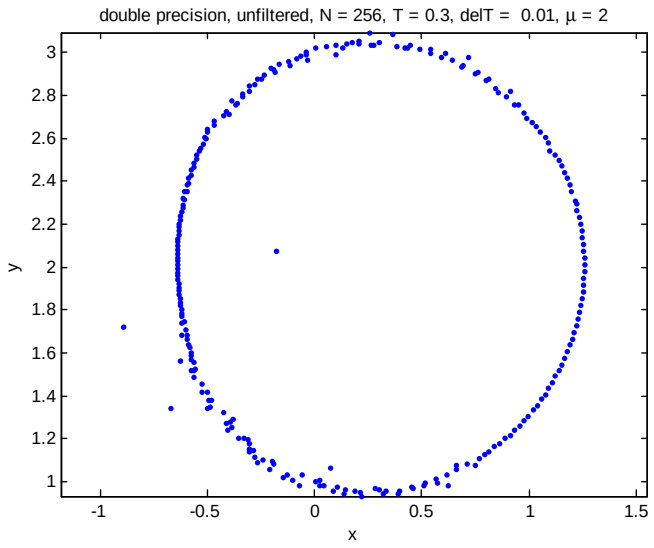
double precision, unfiltered, N = 256, T = 0.3, delT = 0.01, μ = 2
y
x
3
2.8
2.6
2.4
2.2
2
1.8
1.6
1.4
1.2
1
-1
-0.5
0
0.5
1
1.5

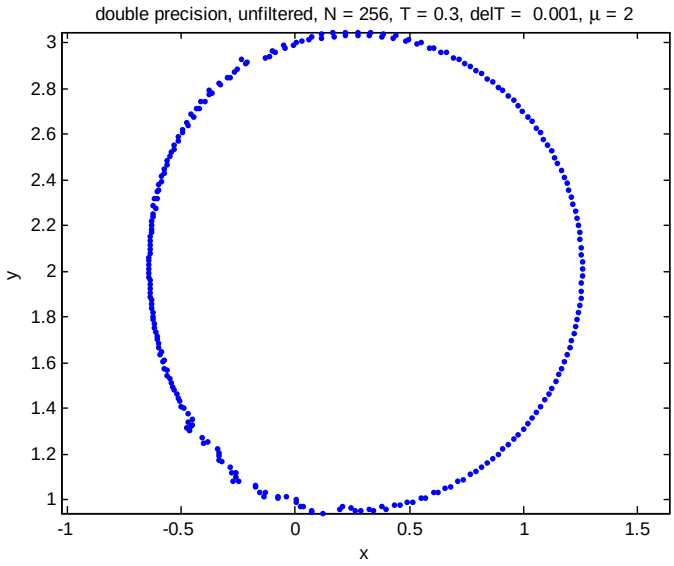
double precision, unfiltered, N = 256, T = 0.3, delT = 0.001, μ = 2
y
x
3
2.8
2.6
2.4
2.2
2
1.8
1.6
1.4
1.2
1
-1
-0.5
0
0.5
1
1.5

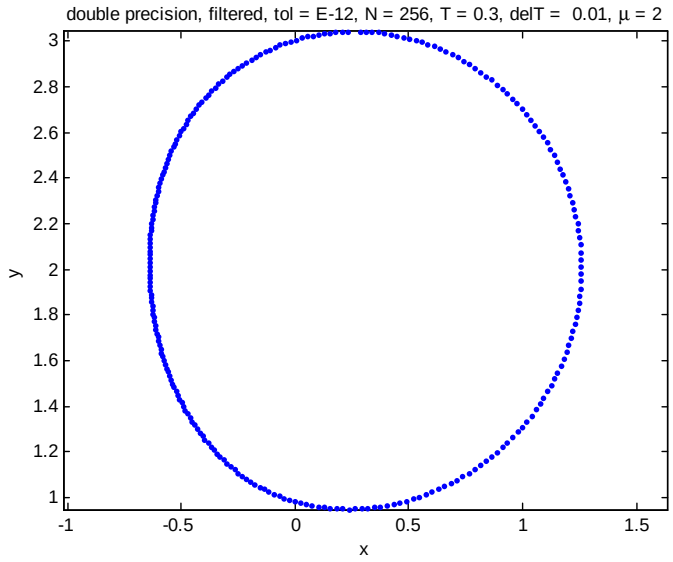
double precision, filtered, tol = E-12, N = 256, T = 0.3, delT = 0.01, μ = 2
y
x
3
2.8
2.6
2.4
2.2
2
1.8
1.6
1.4
1.2
1
-1
-0.5
0
0.5
1
1.5

Chapter 3
Numerical Results

3.1 Evolution of Sheet

Note that from here on in this paper, the fourier filter is implemented, and the computations are performed in double precision. Figure 3.1 shows the evolution of the top vortex sheet, where $N = 512$, $\mu = 2$, filter level $tol = 10^{-12}$, and with a timestep $delT = 0.001$. An explanation of why the sheet rolls up as it does is given by [10]. Observe that the rear of the sheet travels to the right faster than the front of the sheet does.

3.2 Curvature and Estimated Critical Times

The curvature of the vortex sheet is given by $\kappa(\alpha, t) = \frac{x_\alpha y_{\alpha\alpha} - x_{\alpha\alpha} y_\alpha}{(x_\alpha^2 + y_\alpha^2)^{\frac{3}{2}}}$ ([10]). Clearly, for all α, $\kappa(\alpha, 0) = 1$. Figure 3.2 shows the evolution of $\frac{1}{\kappa_{\max}(t)}$. $\kappa_{\max}(\alpha, t)$ denote the maximum curvature at time. The time of singularity formation can be estimated as the time limit in which $\frac{1}{\kappa_{\max}(t)}$ approaches 0. Note that the thus far implemented governing equations are only valid up to the time of singularity formation. Figure 3.2 is a close-up of 3.2, and shows that as the filter level (denoted by 10^{-l} here) and N increase from right to left. Observe that the estimated critical time, the time of singularity formation, decreases as N and l are increased. The critical time can also be seen to decrease as N increases in figure 3.6. Figure 3.6 also shows that the critical time decreases as μ decreases.

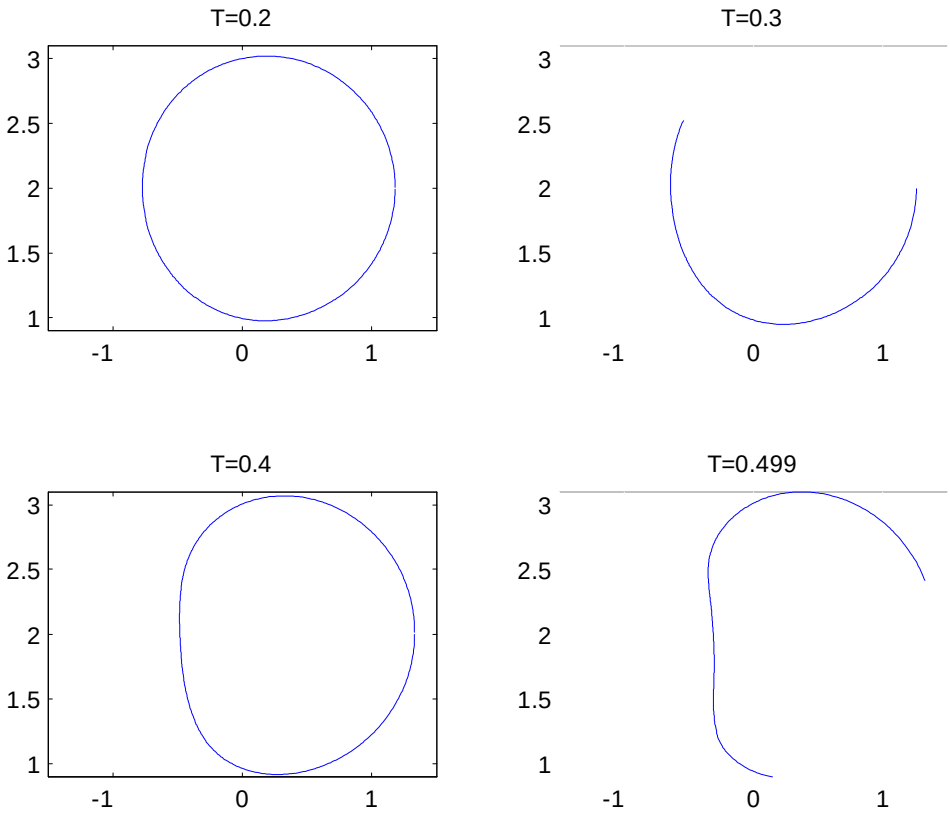

double precision, filtered, tol=E-12, N=512, ΔT=.001, μ=2

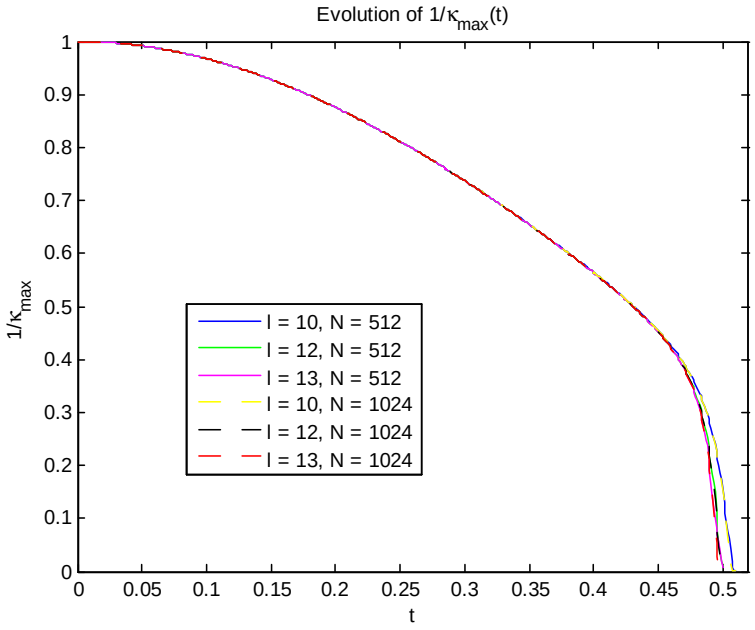

Figure 3.6 illustrates this for $N = 512$. Figure 3.6 provides a close-up of figure 3.6. For $\mu < 1.5$, the critical time seems to decrease linearly as μ is varied. In this region, the slope of the least squares fit is about 0.604. Figures 3.6, 3.6, and 3.6 use the following method to estimate the critical time. If the following two conditions are satisfied [1)] $y_j < c$, for some appropriately chosen constant c (so as to choose a particular region of the sheet), and [2)] $x_j > \max(x_{j+1}, x_{j-1})$, then a singularity has formed in a small neighborhood about (x_j, y_j). This method only roughly approximates the time of singularity formation. Singularity formation is actually predicted a short bit prior to this approximation. The shapes at different critical times are shown in figure 3.6. The point of singularity formation moves down on the actual sheet as μ decreases.

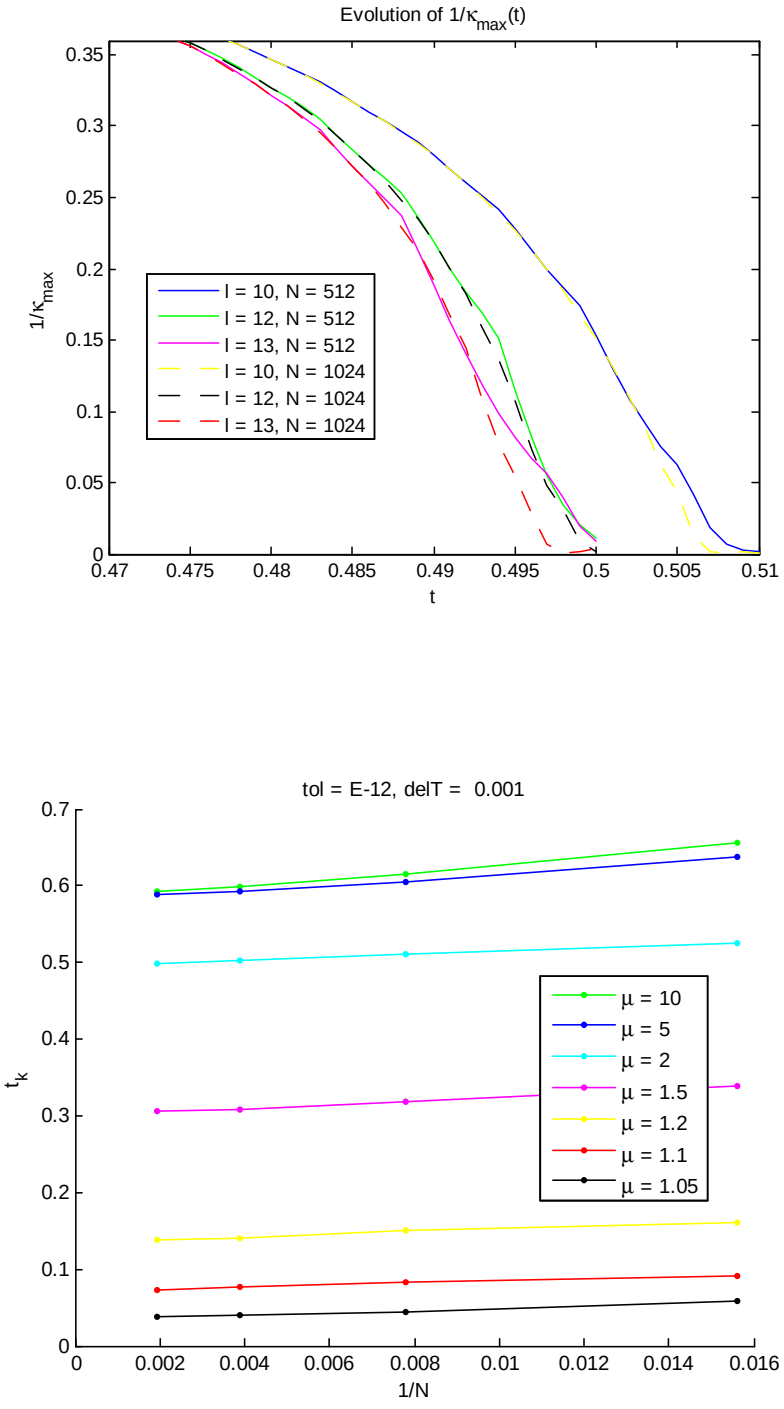

Fig. 3.6. Estimated critical times

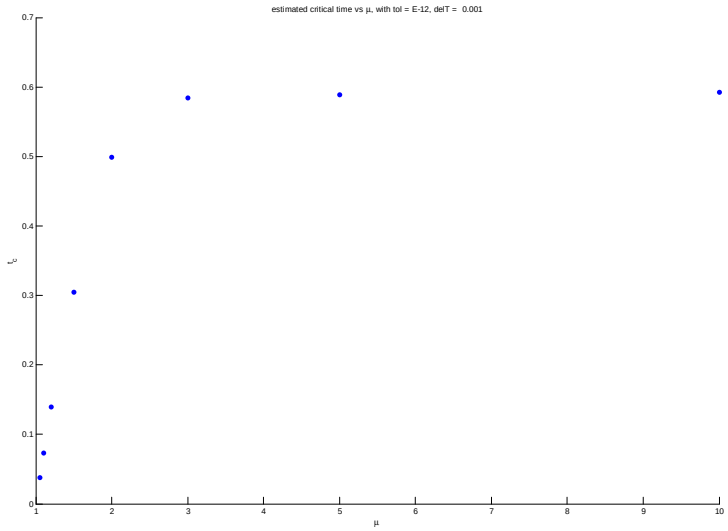
estimated critical time vs μ, with tol = E-12, delT = 0.001
0.7
0.6
0.5
0.4
0.3
0.2
0.1
0
t_c
1
2
3
4
5
6
7
8
9
10
μ

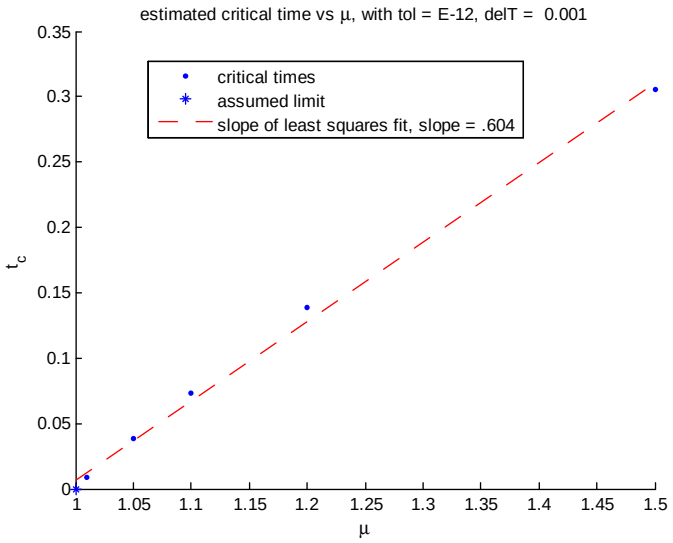
estimated critical time vs μ, with tol = E-12, delT = 0.001
critical times
assumed limit
slope of least squares fit, slope = .604
0.35
0.3
0.25
0.2
0.15
0.1
0.05
0
t_c
1
1.05
1.1
1.15
1.2
1.25
1.3
1.35
1.4
1.45
1.5
μ

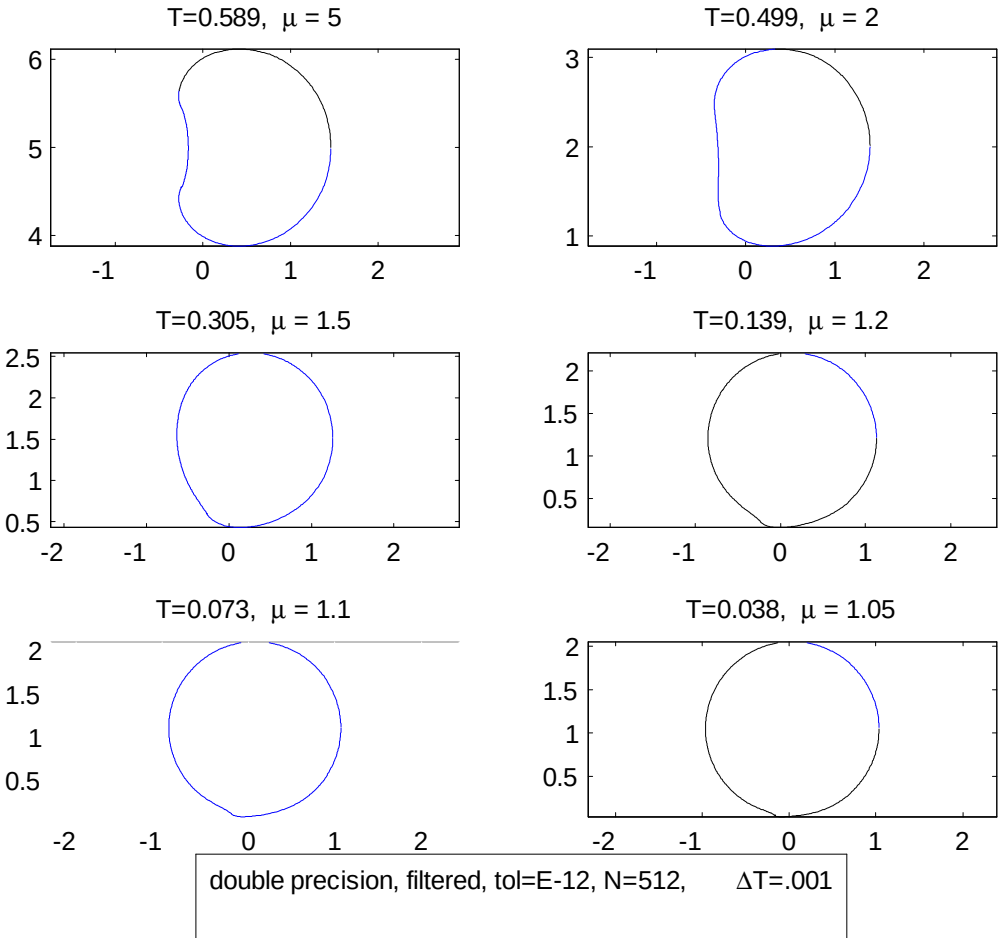
T=0.589, μ = 5
T=0.499, μ = 2
T=0.305, μ = 1.5
T=0.139, μ = 1.2
T=0.073, μ = 1.1
T=0.038, μ = 1.05
double precision, filtered, tol=E-12, N=512, ΔT=.001

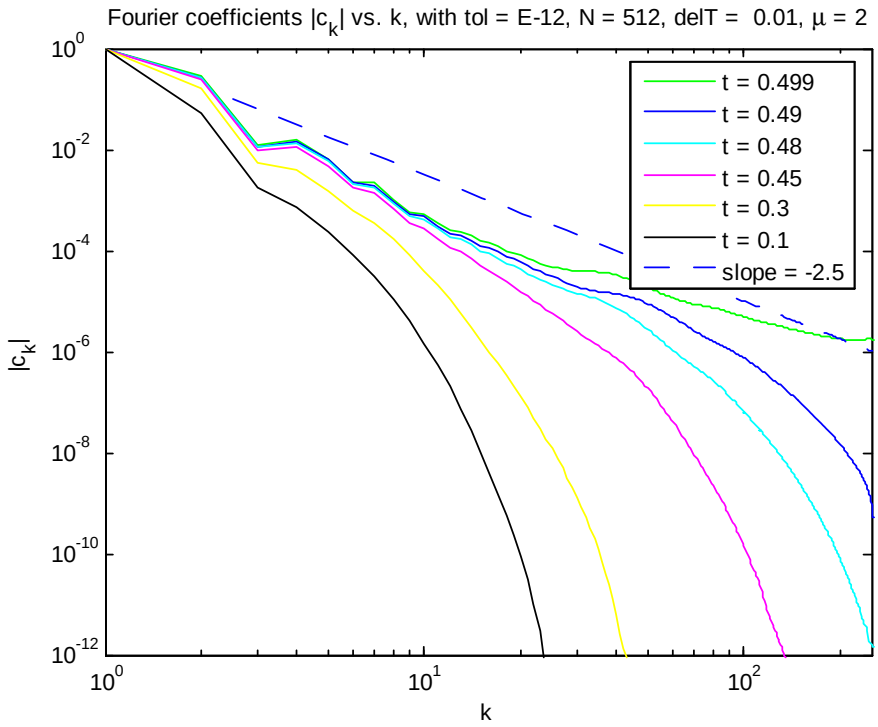

3.3 Type of Singularity

Figure 3.3 shows the absolute value of the fourier coefficients for several different times. As time increases, up to the critical time, the fourier coefficients seem to become linear, with slope -2.5. This line is indicated in the figure. A slope of -2.5 for the fourier coefficients at times near the critical time indicates a branch point singularity with order of $\frac{3}{2}$ [10].

Chapter 4
Conclusion

Note that the numerical methods/governing equations implemented thus far are only valid up to the time of singularity formation. Future work includes performing runs for the mentioned work in quadrapole precision, and performing regularization runs via a method termed the "vortex blob method." The regularization includes putting an artificial δ^2 in the denominator of the principal value integrands. Computation can then proceed past the time of singularity formation. Self shedding and roll-up can then be studied [9]. This method is termed the "vortex blob method." Also, more advanced methods to investigate the branch point singularity with order are sought. After these aims are completed, evolution of the axisymmetric case, which is a toroidal vortex sheet, will be studied and modeled. The mentioned is sought to be completed by August 2007.

.

References

1. Ablowitz, M.J., and Fokas, A.S. *Complex: Introduction and Applications*, 2nd ed. Cambridge University Press, UK, 2003.

2. Chorin, J. C., Marsden, J. E. *A Mathematical Introduction to Fluid Mechanics* 3rd ed. Springer, New York, 2000.

3. David, H.F. and Snider, A.D. Introduction to Vector Analysis, 7th ed. Prentice-Hall, 2000.

4. Krasny, Robert. A Study of Singularity Formation in a Vortex Sheet by the Point-vortex Approximation. *J. Fluid Mech*. vol 167, 65-93 (1986).

5. Krasny, Robert. Desingularization of periodic vortex sheet roll-up. *J. Comp. Phys*. vol 65, no 2, 292-313 (1988).

6. Charles L. Lawson and Richard J. Hanson . *Solving Least Squares Problems*. Prentice-Hall, 1974.

7. Netlib routine. http://www.netlib.org

8. Nitsche, Monika. Math 471: Introduction to Scientific Computing. Course Notes. University of New Mexico, 2006.

9. Nitsche, Monika. Self-similar shedding of vortex rings. *J. Fluid. Mech.* vol 435, 397-407 (2001).

10. Nitsche, Monika. Singularity formation in a cylindrical and a spherical vortex sheet. *J. Comput. Phys.* 173, 208-230 (2001).

11. Saleri, F., and Quarteroni, A. *Scientific Computing with Matlab*. Springer, 2003.